Available online at www.sciencedirect.com
ScienceDirect
Biomaterials 29 (2008) 970–983
Biomaterials
www.elsevier.com/locate/biomaterials

The role of nanometer and sub-micron surface features on vascular and bone cell adhesion on titanium

Dongwoo Khang[a,1], Jing Lu[a,1], Chang Yao[a], Karen M. Haberstroh[a], Thomas J. Webster[a,b,*]

[a]Division of Engineering, Brown University, 184 Hope Street, Providence, RI 02912, USA
[b]Department of Orthopaedics, Brown University, Providence, RI 02818, USA

Received 1 October 2007; accepted 4 November 2007

Abstract

The quantified contribution of pure nanometer (features less than 100 nm in both the lateral and vertical scale) and sub-micron (features larger than 100 nm in the lateral scale) surface structures on the adhesion of vascular (endothelial) and bone (osteoblasts) cells were demonstrated in this study. Compared with flat titanium surfaces, sub-micron surface features led to a 27% increase in surface energy and promoted endothelial cell adhesion density by 200%. In addition, nanometer surface features also led to a 10% increase in surface energy and a 50% increase in endothelial cell adhesion density compared to flat titanium surfaces. Using aligned patterns of such features on titanium, it was clearly identified that both endothelial and bone cells selectively adhered onto sub-micron and nanometer surface features by 400% and 50% more than onto flat regions, respectively. Thus, the surface patterns developed in this study clearly confirmed that sub-micron to nanometer titanium surface features enhanced cytocompatibility properties for both endothelial and bone cells. Although sub-micron features on titanium had the highest surface energy and the greatest cell adhesion densities, nanometer surface features in this study were more efficient surface features increasing both surface energy and cell adhesion more with respect to smaller changes in surface area and surface roughness (compared to sub-micron surface features on titanium which had considerably larger changes in surface area and surface roughness).

Keywords: Vascular; Bone; Sub-micron surface roughness; Surface energy; Nano-surface roughness; Titanium

1. Introduction

Traditionally, titanium-based materials have been considered as durable and biocompatible implant materials for both vascular and orthopedic applications [1–3]. The problem with current drug-eluting titanium stents lies in the fact that immunosuppressant drugs placed in a polymer coating on titanium stents also inhibits the proliferation of vascular endothelial cells (cells that naturally cover the interior of a healthy blood vessel) [4,5]. Although such inhibition caused by drug elution on vascular cells does not happen on bare titanium stents, sometimes bare titanium stents cause poor bonding with the endothelium or cause extensive inflammatory responses which further limit endothelialization [6]. For this reason, maximizing initial endothelial cellular adhesion and reducing inflammatory immune responses with titanium stent surfaces by altering intrinsic surface properties (such as topography, roughness and energy) are, thus, extremely important factors in the design of future vascular stents [5,7].

A similar situation has been reported for titanium used in orthopedic applications. It has been reported that almost 25% of all hip implant surgeries performed today require revisions to retrieve a failed titanium implant [8]. This is because the average functional lifetime of today's orthopedic titanium implants ranges only from 10 to 25 years; clearly additional orthopedic surgery (after 10–25 years) is a large burden for any patient [9]. One of the major causes of titanium implant failure involves incomplete osseointegration (or bonding of the implant to surrounding bone)

*Corresponding author at. Division of Engineering, Brown University, 184 Hope Street, Providence, RI 02912, USA. Tel.: +1 401 863 2318; fax: +1 401 863 9107.
E-mail address: Thomas_Webster@Brown.edu (T.J. Webster).
[1]Contributed equally.

0142-9612/$ - see front matter © 2007 Elsevier Ltd. All rights reserved.
doi:10.1016/j.biomaterials.2007.11.009

and, thus, it is currently believed that early sufficient formation of new bone on a titanium orthopedic implant surface will quickly fix the implant into juxtaposed bone ensuring a longer functional lifetime [10–12].

In this respect, bio-inspired nano-materials (with surface structures less than 100 nm) can be essential to resolving current problems associated with titanium-based vascular and orthopedic implant materials [7,13,14]. This is because desirable cellular responses on nano-structured titanium can lead to a stronger initial bio-integration with surrounded tissue to increase both the lifetime and bonding between appropriate tissues and implant surfaces.

However, previous reports have been unclear towards the contribution of nanometer surface roughness of implants on cell functions because such materials also change in their surface chemistry [13,15–18]. For example, one way to formulate nanometer features on titanium is through anodization in which both chemistry and surface roughness are altered due to increases in the percentage of oxygen on titanium surfaces. This makes it difficult to quantify the independent contribution of anodized nano-porous structures on titanium versus chemistry changes at promoting bone cell functions [16]. In addition, most of these surface structures are meta-structure systems composed not only of nanometer surface structures (features less than 100 nm in both the lateral and vertical scales) but also of sub-micron scale structures (especially those larger than 100 nm in the lateral or vertical scale). Therefore, it has been unclear whether specifically small nanometer surface structures (less than 50 nm in the lateral and vertical scales) is a meaningful contributing factor for enhancing tissue-forming cell responses.

To answer the above question, three different surface structures (flat, nanometer and sub-micron) were created in the present study with identical titanium chemistry to analyze endothelial and bone cell adhesion. In addition, altered surface properties (such as surface energy, surface area difference and surface roughness) were characterized and correlated to the various surface features created (using atomic force microscopy (AFM) and a contact angle analyzer).

In addition, highly aligned micron patterns featuring two different surface structures (flat, nanometer or sub-micron) on titanium were manipulated to determine the spatial adhesion difference of bone and endothelial cells. The advantage of this novel aligned substrate is that it can simultaneously determine different cytocompatibility properties of nanometer and sub-micron titanium structures on cell adhesion and, thus, can serve as a quick assay for determining cytocompatibility properties of the designed materials.

In this manner, the objective of this *in vitro* study was to modify the size of titanium surface features of identical chemistry from flat to sub-micron to nanometer scale and compare initial endothelial and bone cell adhesion on such surfaces. Furthermore, different titanium surface structures were aligned (with micron spaces) to determine the possible selective and spatial control of endothelial and bone cell adhesion.

2. Materials and methods

2.1. Generating nanometer and sub-micron Ti roughness

Pure titanium (99.8% of purity: T-2069, Cerac Inc.) was deposited on glass coverslips (12-550-15, Fisher-Scientific, NH) with 50 nm of thickness using an e-beam evaporator (in a vacuum state: 10^{-7} Torr, Fig. 1a) to generate flat titanium surfaces (labeled as R-1). The default e-beam deposition rate used in this experiment was 2 Å/s with an e-beam current density of 60–70 mA/cm^2 (R-1 in Fig. 1a). Previous studies have generated rough surfaces by altering the deposition parameters using an ion-beam deposition process [19,20]. In this study, a high deposition rate (20 Å/s with an e-beam current density of 130 mA/cm^2) was used to generate nanometer surface topographies with a deposition of 50 nm thickness on R-1 (defined as R-2 in Fig. 1b). In addition, to generate sub-micron surface features, the same e-beam current density was used with a deposition of 1 μm thickness on R-1 (defined as R-3 in Fig. 1b). The e-beam energy was set to 7 keV during the experiments.

2.2. Highly aligned patterns of flat, nanometer and sub-micron surface roughness

For generating two different titanium roughness values (i.e., those either flat and nanometer or flat and sub-micron) on one substrate, an aligned shadow mask or conventional grid (G-400P-Ni, Electron Microscopy Sciences, PA) was used to block titanium deposition from the e-beam which allowed for the deposition of titanium nanometer particles only in open spaces (Fig. 1c). Then, nano-structured titanium particles (obtained by a high current e-beam) were deposited within the aligned open spaces and this, thus, generated two different surface roughness features (Fig. 1c). The advantage of this method is that it allows one to generate different patterns (with different sizes of surface features) on one substrate by altering the deposition parameters (as described in Section 2.1).

2.3. Surface chemistry and topography characterization (FESEM, EDS and AFM)

Field emission scanning electron microscopy (FESEM, LEO 1530 VP) was used to investigate the surface morphology of the thin film surfaces including flat, nanometer and sub-micron structured titanium (at 5–7 kV with 10,000 ×).

Chemical composition of specific regions (R-1, R-2 and R-3) on substrates was examined by energy-dispersive spectroscopy (EDS) using an Oxford INCA 250 detector and associated software (Oxford Instrument America, Inc., Concord, MA).

Nanometer surface roughness measurements were completed using a multimode AFM (Dimension 3100, Veeco, CA) to compare flat, sub-micron and nanometer surface features. Scan areas of both 5 μm × 5 μm (sub-micron resolution) and 500 nm × 500 nm (nanometer resolution) were used to analyze sub-micron and nanometer scale surface features. Commercially available AFM tips (radius of tip curvature was less than 10 nm, NSC15/ALBS, Micro-Masch, OR) were used in tapping mode with a scan rate of 0.5 Hz. Full tip cone angles were 30° but less than 10° at the 200 nm tip apex (tip height was 25 μm with a 40 N/m of force constant). Note that all of the vertical surface features did not exceed 200 nm (Figs. 2a–f), so negligible convolution effects (from the tip) were anticipated. Surface area was calculated as a summation of triangles over the surfaces of the analyzed area (5 μm × 5 μm), which was defined by two-by-two pixel kernels (Veeco, Technical Manual).

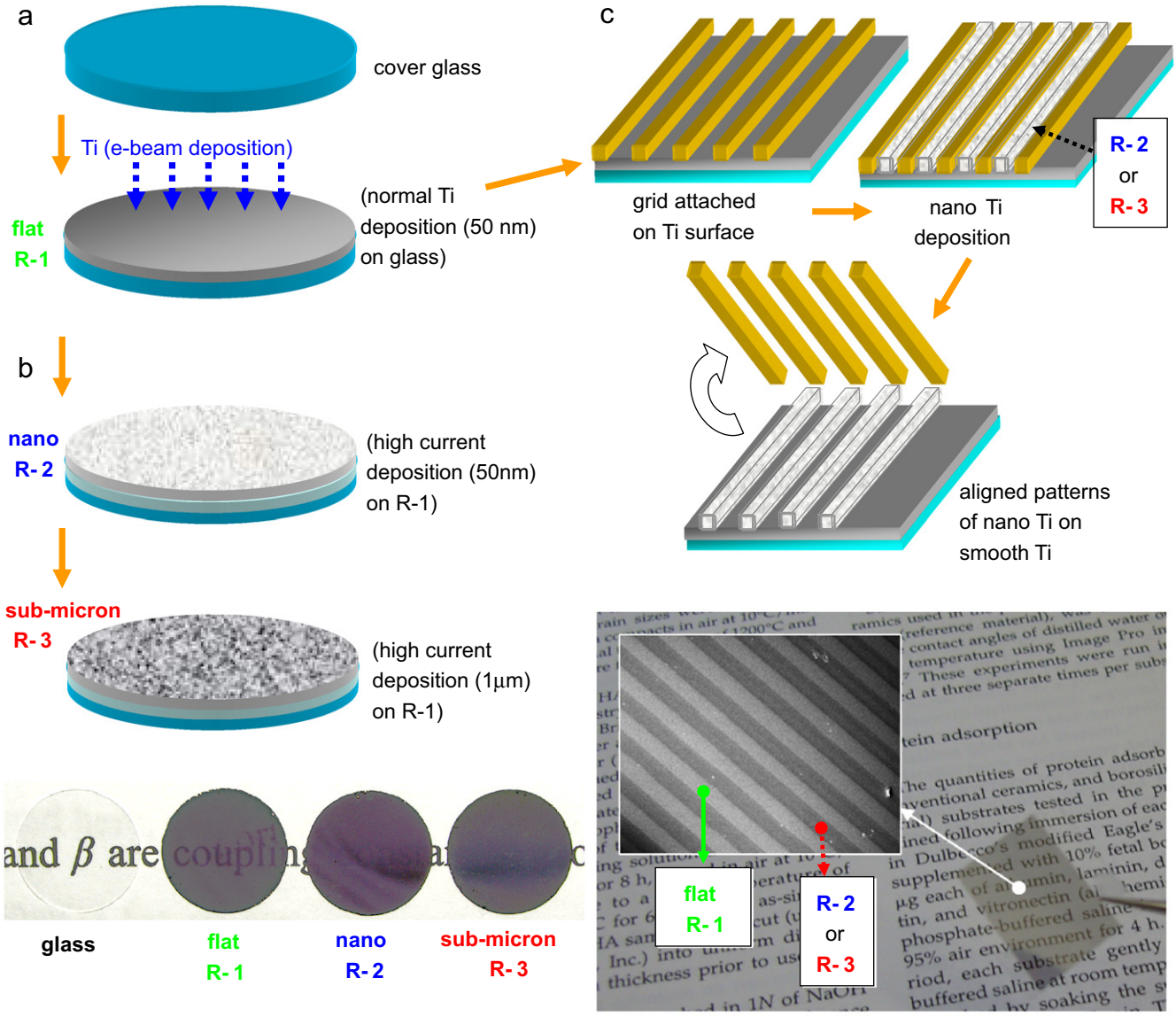

Fig. 1. Fabrication of flat, nanometer and sub-micron surface roughness on bulk and aligned titanium surfaces. (a) A conventional e-beam deposition rate (2 Å/s) generated flat titanium (R-1) surfaces on glass coverslips (50 nm of thickness). (b) A high e-beam deposition rate (20 Å/s) generated nanometer surface roughness (R-2) after a thickness of 50 nm on R-1. High deposition rates with a thickness of 1 μm generated sub-micron surface structures (R-3). The inset image showed different transparency for these substrates because of the different deposition thickness on glass coverslips. Sub-micron titanium surfaces were opaque. (c) Schematic of aligned micron patterns of different surface roughness (sub-micron, nanometer surface or flat). A titanium thin layer (50 nm) on glass coverslips was used as a base substrate. A metal grid (Ni/Au/Cu or shadow mask) with aligned grooves (width of 30 μm) was placed on the R-1 (see (a)). Nanometer or sub-micron rough titanium was coated through the open grooves (respectively) as described in (a) and (b). Then, the shadow mask was removed from the R-1 to generate aligned patterns of two different surface roughness values on titanium. The inset image showed that the aligned titanium patterned surfaces were still transparent (SEM image shows aligned patterns with 30 μm spaces: aligned dark regions are nanometer or sub-micron layers and bright regions correspond to flat surfaces (R-1)).

2.4. Surface energy and contact angles

A drop shape analysis system (Easy drop contact angle system, Kruss, Germany) with analysis software (DSA1) was used to determine the surface contact angles on the titanium samples. Distilled water was used as a contacting solvent. All data were obtained 5 s after placing the droplet on the surfaces under ambient conditions. For the surface energy calculation, $E_s = E_{lv}\cos\theta$ was used where $E_{lv} = 72.8\,mJ/m^2$ at 20 °C for pure water and θ is the static contact angle [21]. Here E_s is the surface energy of the contacting surface and E_{lv} is the surface energy between the water and air under ambient conditions.

2.5. Cell culture

Two important tissue-forming cells, vascular (specifically, endothelial cells) and bone cells (osteoblasts), that interact with titanium, were used in this study. For the endothelial cell culture, rat aortic endothelial cells (RAEC) were used (VEC Technologies, passage numbers 5–10). Petri dishes were coated with 0.2% gelatin (Sigma) for 2 h at room temperature for culturing, followed by air-drying in a laminar flow hood for 12 h. RAEC were then cultured in complete medium (MCDB-131, VEC Technologies) under standard cell culture conditions (37 °C, humidified, 5% CO_2/95% air environment). Medium was replenished every other day during cell culturing.

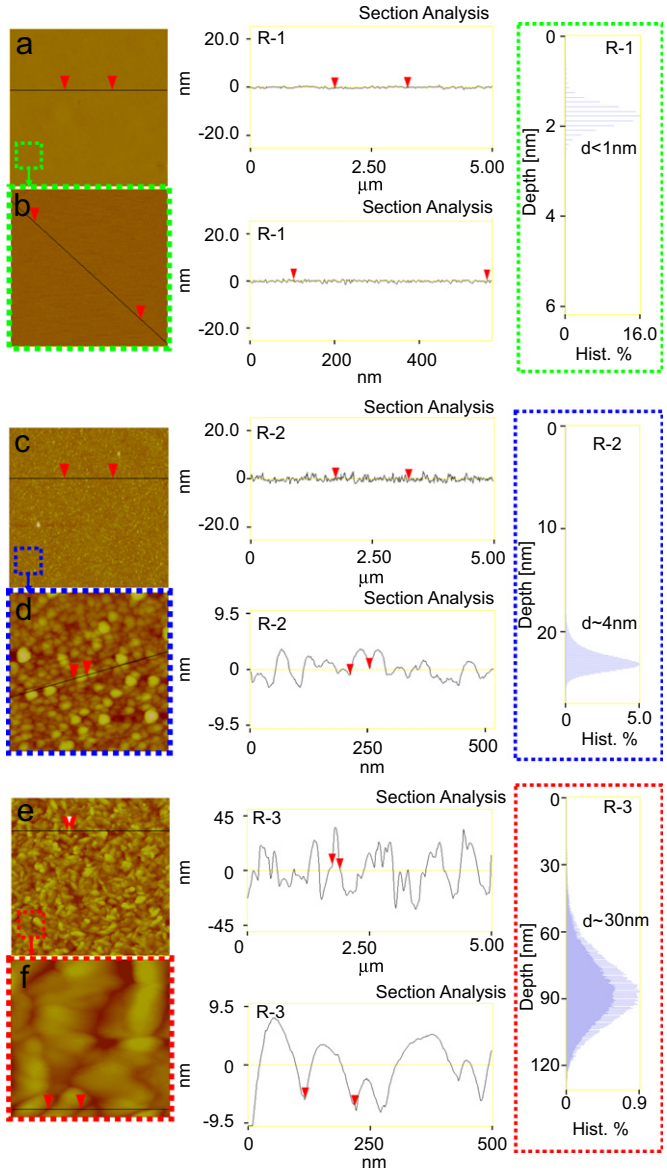

Fig. 2. AFM characterization. (a)–(b) AFM analysis of R-1 showed no surface features at the sub-micron and nanometer scale. A sectional analysis showed that R-1 had flat (or smooth) structures in both the nanometer and sub-micron scales. Depth analysis (inset image) showed negligible hits of depth features (less than 1 nm). (c)–(d) AFM analysis showed clear differences in surface features at the sub-micron and nanometer scales. AFM sectional analysis showed that R-2 (nanometer surface features) had very rough surface features at the nanometer scale (structure widths were 30–40 nm) whereas surface roughness at the sub-micron scale was less. Depth analysis (inset image) showed that a majority of hits were distributed within 2–6 nm. (e) AFM analysis showed that R-3 had very rough surfaces at the sub-micron scale but it had rather smooth surface structures at the nano-scale: less lateral scale variation compared to R-2 in the nanometer scale in (f). The widths of lateral structures were above 100 nm. Depth analysis (inset image) showed that the depth of titanium surface sizes were around 20–40 nm. All depth profiles were measured from 5 μm × 5 μm of AFM scan area.

For bone cell experiments, human osteoblasts (HOB, CRL-11372, ATCC, population numbers 2–5) were cultured under standard cell culture conditions (i.e., a 37 °C, humidified, 5% CO_2/95% air environment) and were cultured in Dulbecco's modified eagle medium (DMEM, Gibco), supplemented with 10% fetal bovine serum (FBS, Hyclone) and 1% penicillin/streptomycin (P/S, Hyclone), under standard cell culture conditions.

2.6. Cell adhesion assay

For the endothelial cell adhesion test, RAEC were seeded at a density of 3500 cells/cm^2 on non-patterned (bulk) titanium surfaces. In addition, for cell adhesion tests on patterned (aligned with 30 μm spaces) titanium surfaces, HOB and RAEC were seeded at a density of 5000 cells/cm^2. Both cells were incubated for 4 h under standard cell culture conditions.

After 4 h, non-adherent RAEC cells were removed by rinsing in PBS. Cells were then fixed with 4% formaldehyde (Fisher) at the end of the time period (4 h) and were counted by staining with Rhodamine Phalloidin (R415, Molecular Probes) to visualize F-actin filaments as well as a Hoechst dye (33258, Sigma) to visualize the cell nucleus. To investigate altered endothelial cell morphology on the different titanium features (i.e., flat, nanometer and sub-micron), aspect ratios (cell length/cell width) for each cell was calculated.

For adhesion tests for osteoblasts, non-adherent HOB were removed by rinsing in PBS while adherent HOB viability was determined by a LIVE Viability/Cytotoxicity Kit (Molecular Probes). Briefly, the cells were stained with 3.3 μM of calcium AM and 1.7 μM of ethidium homodimer-1 and incubated for 30 min before visualization using fluorescence microscopy (Axiovert 200M, Zeiss) which was equipped with a sensitive monochrome camera (Hamamatsu ORCA-ER). The live cells on the aligned patterned titanium surfaces were counted at 530 nm (excitation for calcein AM) and 560 nm (ethidium homodimer-1) wavelengths using a fluorescence microscope.

For the quantification of HOB, Hoechst dye (33258, Sigma) was used to visualize the HOB nucleus. HOB morphology on the aligned substrates (after 4 h) was also examined using SEM. For SEM investigation, HOB were fixed (after 4 h) with formalin for 5 min and then, they were dehydrated by soaking serially in 10%, 30%, 50%, 70% and 90% ethanol for 30 min followed by soaking in 100% ethanol for 15 min (three times). Lastly, the substrates were critically point-dried for SEM visualization.

2.7. Statistical analyses

All experiments were conducted in triplicate and repeated at three different times. Experimental data were analyzed statistically using ANOVA (with single factor) and commercially available programs: Excel (Microsoft, WA) and Origin 7.5 (Origin Lab, MA).

3. Results

3.1. Nanometer and sub-micron Ti surface roughness

Fig. 2 demonstrates the nanometer and sub-micron surface features obtained in this study on titanium. A normal e-beam deposition rate generated flat surfaces on a cover glass. AFM sectional analysis indicated no structural variation in both micron and nanometer scales (Figs. 2a and b). The inset image (depth analysis) also showed negligible depth (vertical) hits (signals due to any height difference due to surface features). These results mean that there were no meaningful features for both vertical and lateral scales for the flat titanium surfaces.

High e-beam current densities (see Section 2.1 for details) generated tiny surface features (deposition of 50 nm) at the sub-micron scale (Fig. 2c). Interestingly, Figs. 2c and d showed more distinct surface features at the nano-scale than sub-micron scale. Sectional analyses

clearly showed visible nanometer surface structures (R-2: structures were 30–40 nm in the lateral and 2–6 nm in the vertical scales). Since both vertical and lateral structures were less than 50 nm, all the surface roughness that came from these features should be considered as pure nanometer surface roughness. The vertical depth (inset images of R-2) profile also showed that most of the AFM depth hits were obtained from 2 to 6 nm with a distribution of most features at 4 nm.

Figs. 2e and f showed very drastic differences of surface roughness (both lateral and vertical) between the sub-micron and the nano-scale titanium surfaces. In contrast to previous increased surface roughness at the nano-scale than at the sub-micron scale (R-2: Figs. 2c and d), a high current density of e-beam deposition with a thickness of 1 μm generated very rough surface features (both lateral and vertical) at the sub-micron scale (R-3: Fig. 2e). However, at the nano-scale (Fig. 2f), those structures were relatively smooth compared to R-2 in the lateral scale (Fig. 2d). This clearly demonstrates that sub-micron scale surface features (larger than 100 nm in lateral width) were dominant on R-3 surfaces (but vertical structures were still less than 100 nm). The reason for altered surface structures in R-3 (compared to R-2) can be anticipated since the higher deposition thickness generated many layers of titanium nanometer particles and, thus, caused the surface structures to be more smooth at the lateral scale but increased roughness at the vertical scale (at the nanometer scale). The depth of R-3 (inset image) also showed increased vertical structures (0–70 nm) with a distribution of maximum titanium surface features within 30–40 nm (in the vertical scale).

Interestingly, the above developed titanium samples had altered transparency. This was due to the different deposition thickness generating not only different sizes of surface features on titanium, but also different transparencies of each sample (inset image of Fig. 1b). The glass, flat titanium (50 nm deposition of titanium) and nanometer titanium structures (100 nm deposition in total) were still transparent (although the transparency was very low compared to flat structures) under standard illumination. However, sub-micron structured surfaces were completely opaque because of the high deposition thickness (1 μm) of titanium (Fig. 1b). The aligned titanium patterns (30 μm for each pattern) of the two different surfaces were also transparent under normal illumination (inset image of Fig. 1c).

3.2. Highly aligned patterns (different surface roughness) of Ti with identical surface chemistry

FESEM images showed that the method developed in this study successfully generated two different surface features for aligned patterns (Figs. 3a–e). Fig. 3a showed aligned patterns of R-2 (nanometer surface features) with R-1 (flat surface features) after deposition of 50 nm thick titanium. The high magnification SEM of R-2 in Fig. 3a demonstrated nanometer and flat surface structures (inset images) as observed in Figs. 2b and c.

High deposition thickness (1 μm) generated clear differences in R-3 and R-1 at low magnifications (Fig. 3b). The magnified SEM image of R-3 demonstrated drastic increments in surface features at the sub-micron scale (as already verified in Fig. 2e). These facts suggested that SEM alone cannot be a scanning tool for analyzing pure nanometer surface features (specifically, features less than 50 nm in the width and depth scales) although sub-micron surface features can be analyzed by conventional FESEM.

The AFM depth profile image provided evidence that height differences between the upper and bottom layers (R-3 and R-1) of titanium were about 1 μm (Figs. 3c and d). AFM section analysis also showed two different surface roughness values (R-3 and R-1: Figs. 3d and e).

Surface chemistry results (EDS) provided no significant evidence of differences in surface chemistry between each surface (i.e., flat, nanometer and sub-micron; see Table 1 for details). This was anticipated since the source of titanium was pure (99.8%) and was evaporated in a high vacuum state (10^{-7} Torr).

3.3. Increased surface energy on sub-micron and nanometer-structured surfaces

The size of surface features in both the nanometer and the sub-micron scale altered water contact angles on titanium (Figs. 4a–c). In summary, flat titanium surfaces (R-1) were hydrophilic (water contact angles less than 45°). However, the nanometer surface rough titanium (R-2) was more hydrophilic (contact angles were less than 32°) compared to flat titanium surfaces (Fig. 4b: R-2). This means that small nano-sized surface features on titanium (RMS values less than 2 nm, 40 nm lateral width and 4 nm vertical depth achieved on 50 nm titanium thin films) altered water contact angles by more than 10° compared to flat titanium (R-1) surfaces (Fig. 4e). This result is very intriguing since small changes in surface area (0.7% increment) led to 10% increases in surface energy compared to flat titanium.

Water contact angles showed even greater hydrophilicity on sub-micron titanium surfaces than nanometer titanium surfaces (R-3: contact angles were less than 20° which corresponded to 70 mJ/m^2: see Fig. 4e). Although sub-micron surface roughness did not generate such a large increment in surface energy with respect to altered surface area (30% increase in surface energy with a 6% increase in surface area) as nanometer titanium surface roughness did (10% increase in surface energy with a 0.7% increase in surface area), RMS values as measured by AFM for sub-micron features drastically increased (more than 10 nm; see Fig. 4d) due to increased vertical depth (Figs. 2e and f and inset vertical depth hits) compared to nanometer titanium surfaces (Figs. 2c and d and inset vertical depth).

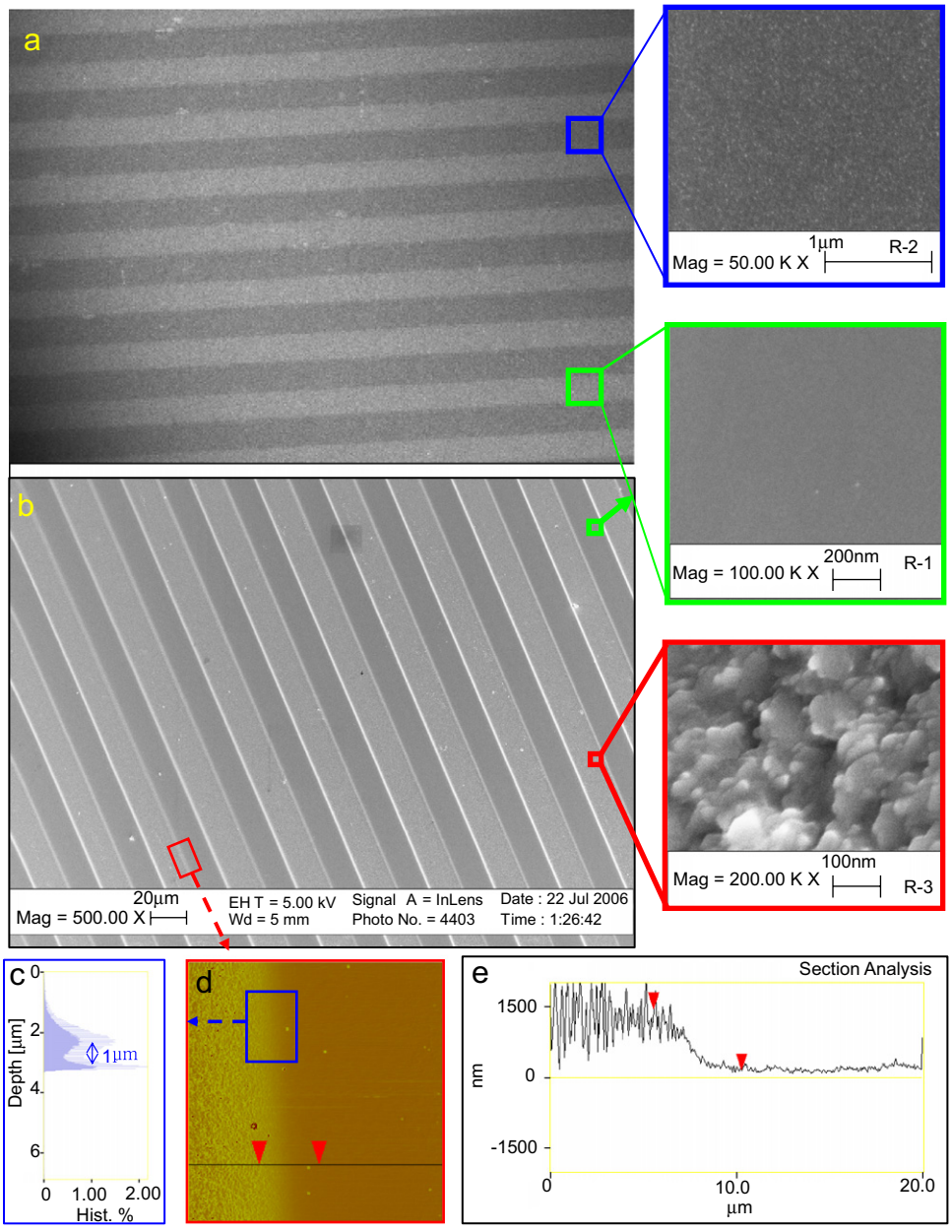

Fig. 3. SEM characterization. (a) Highly aligned micron patterns of nanometer structures (R-2) on flat titanium (R-1). Inset image (upper) showed the surface spots due to the nanometer scale surface structures (R-2): those structures were already observed in Fig. 2c. The flat region (below inset) did not show any surface structures at the nanometer scale. (b) Highly aligned micron patterns of R-3 (sub-micron titanium) on flat titanium (R-1). Inset magnified images show a very rough morphology of R-3 in the sub-micron scale. (c)–(d) Depth analysis showed the height difference between R-3 and R-1 and the difference was about 1 μm (confirmed deposition thickness). (d)–(e) AFM analysis at the aligned intersection between R-3 and R-1. (e) AFM sectional analysis of (d) showed two clear differences in surface roughness (flat and sub-micron).

3.4. Endothelial and osteoblast cell adhesion

Fig. 5 showed greater adhesion of RAEC on bulk R-3 compared to R-1 (Figs. 5a–e). Importantly, RAEC densities increased on sub-micron and nanometer surface features about 216% and 58%, respectively, compared to cell density on flat titanium surfaces (Fig. 5e). Magnified images of cell body staining (F-actin) clearly showed different aspect ratios of RAEC on R-3 (sub-micron structures) compared to smooth titanium surfaces (Fig. 5f). This is consistent with recent results [5,7] that a majority of RAEC of increased aspect ratios adhered onto sub-micron than smooth surface features. Since most of the endothelial cells in the natural inner blood vessels are aligned with blood flow, as determined by cell morphology aspect ratios, sub-micron scale surface features showed more favorable endothelial cell attachment than flat titanium surfaces.

In addition, RAEC adhesion on aligned patterns showed that more than 80% of RAEC selectively adhered onto

Table 1
EDS analysis for flat, nanometer and sub-micron Ti surfaces

Element	Weight (%)	Atomic (%)
Si K	1.72 (±0.024)	2.91 (±0.036)
K K	0.68 (±0.012)	0.82 (±0.012)
Ti K	97.22 (±0.331)	96 (±0.2)
Totals	100.00 (including error)	

There were no significant changes in surface chemistry for flat, nanometer and sub-micron structured surfaces (errors were ±0.031%). Some Si and K signals were noticed due to the presence of the glass substrate beneath the titanium deposition.

sub-micron titanium patterns (dark regions compared to bright patterns in Figs. 6a and b). Results clearly showed RAEC F-actin filaments tended to orient on the sub-micron features compared to flat regions (Fig. 6b).

In addition, 65% of RAEC selectively adhered onto nanometer surface-featured titanium patterns (R-2) compared to flat surfaces (Fig. 6c). To determine if the selective adhesion of RAEC came from altered surface properties (surface roughness and surface energy), similar height layers (50 nm and 1 μm in height difference) with the same surface properties (both layers were flat) were tested for RAEC adhesion but showed no preferential adhesion on the top and bottom layers (Fig. 6d). This clearly verified again that the selective adhesion of RAEC (R-2 or R-3) was due to the presence of nanometer and sub-micron surface features, not due to height differences between the two layers. In conclusion, aligned titanium patterns with different surface features demonstrated clear evidence that sub-micron and nanometer surface roughness led to selective RAEC adhesion although identical surface features on both layers (top and bottom) did not lead to any selective RAEC adhesion (both on the bottom and on the top layers. See Fig. 6e for detail).

HOB adhesion on aligned titanium patterns clearly showed more adhesion on sub-micron structured layers (R-3: dark patterns in Figs. 7a and b) than flat titanium (R-1: bright patterns compared to R-3 in Figs. 7a and b). SEM images showed various HOB adhesion on aligned patterns on different surface features (R-3 and R-1 in Figs. 7c–e). Some adherent HOB preferred to attach on R-3 or at the intersection of R-3 and R-1 (Fig. 7d). This can be interpreted that surface structures at those intersections (R-3 and R-1) have moderate slopes (few μm) with high surface roughness and, thus, induced cell adhesion at the cross-section between R-3 and R-1 (see surface features in Figs. 3d and e). Statistical analysis showed that most of the HOB selectively adhered on R-3 (more than 80%) compared to R-2 (more than 60%) versus adhesion on R-1 (Fig. 7f). This selective adhesion may be due to the high-surface energy (about 70 mJ/m^2), which provided more optimal protein interaction [22] to mediate of HOB adhesion than nanometer (62 mJ/m^2) and flat titanium surfaces (54 mJ/m^2: see Fig. 5f).

3.5. Role of sub-micron and nanometer surface structures on cell adhesion

Fig. 8 shows the correlation between the adhesion probability of RAEC cells and various surface features with respect to altered width and depth. Depending on the values of the width and depth, surface structures were defined by flat, nanometer and sub-micron surfaces (R-1, R-2 and R-3). Based on Fig. 5, RAEC adhesion increased 50% on nanometer titanium surface features compared to flat (R-1) titanium surfaces. Also, RAEC adhesion densities on sub-micron structures (R-3) increased 200% compared to flat titanium. In addition, RAEC increased 40% on sub-micron features compared to nanometer-featured titanium. A majority of R-3 features in the lateral dimension were larger than 100 nm although vertical depths of sub-micron titanium structures (R-3) were below 100 nm (Fig. 8a). Since altered lateral widths of nanometer surface features were almost 10 times higher than the altered vertical structures, an increase in lateral widths was considered as a meaningful factor for altered surface energy (Fig. 8b). Especially, it is impressive that altered lateral nanometer dimensions (about 40 nm) led to drastic changes in surface energy (10% increment just from 0.7% increased surface area compared to flat surface) and induced greater cell adhesion (50% in Fig. 8c). This might be due to altered titanium nanometer topography (increased lateral width of surface features) inducing more spreading (greater wettability or surface energy) with enhanced cell adhesion than flat titanium surfaces of identical chemistry [23,24]. It was assumed that altered vertical structures (about 4 nm) did not lead to a drastic impact on increases in surface energy and cell adhesion because greater vertical depths led to lower surface energy and decreased cell densities as observed by previous studies [15,24,25]. Also, altered vertical depths (4 nm) were negligible compared to altered lateral dimensions (40 nm). However, a more rigorous study needs to focus on understanding the altered surface properties with respect to subsequent cell adhesion. Importantly, in this analysis, it was clearly identified that small nanometer surface titanium roughness (due to nanometer scale surface features) resulted in a drastic increase in surface energy (an important factor for cell adhesion) that led to the subsequent

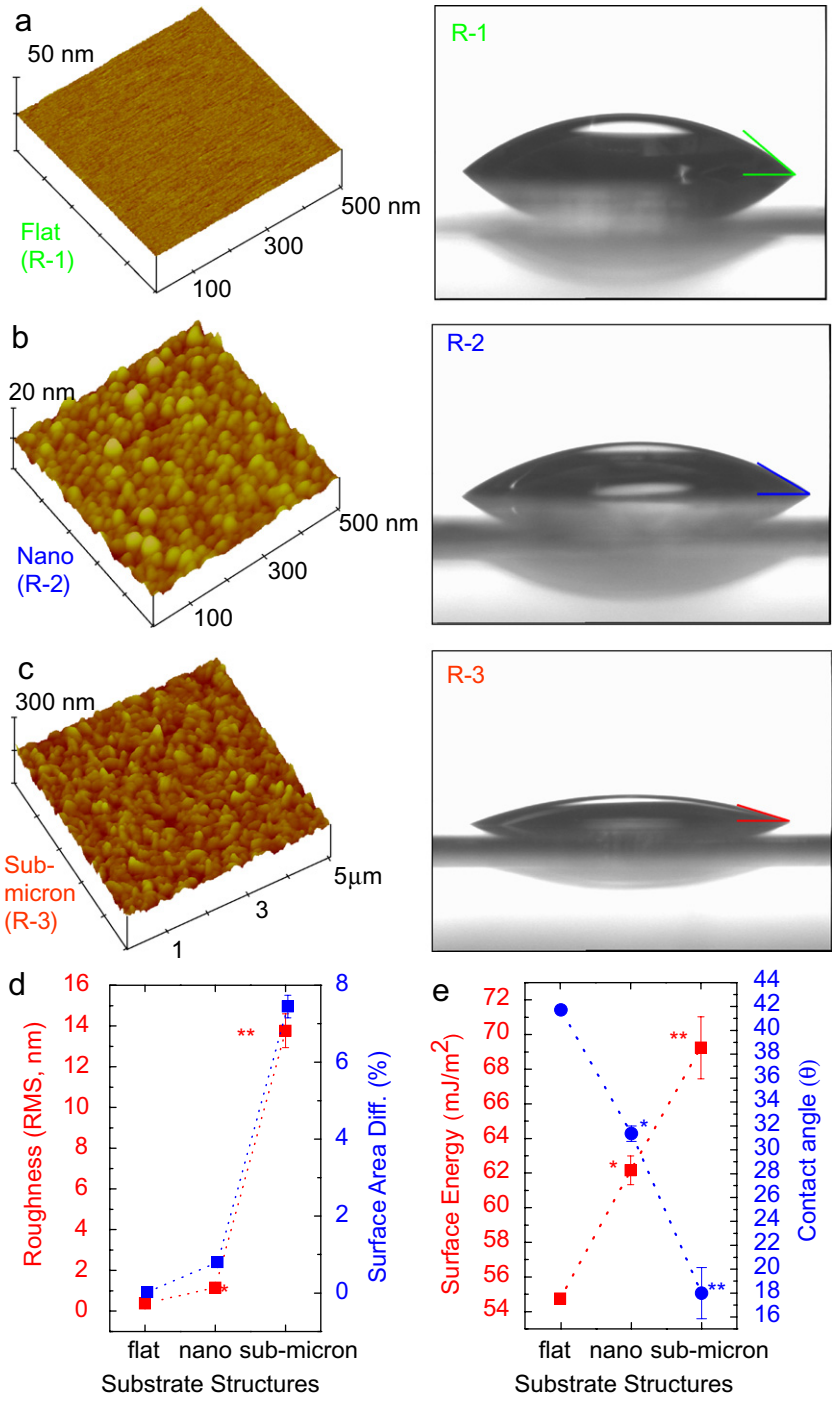

Fig. 4. Greater surface roughness, area and energy. Contact angles showed increased hydrophilicity on (a) flat, (b) nanometer and (c) sub-micron (increasing from left to right) surface-featured titanium. (d) Surface roughness (RMS) and surface area (%) showed negligible differences between R-1 (flat) and R-2 (nanometer: 0.7%) but R-3 (sub-micron) showed increased RMS (more than 10 nm) and increased surface area by 7% compared to flat surfaces. (e) Compared to flat (54 mJ/m^2), nanometer (62 mJ/m^2) and sub-micron (69 mJ/m^2) titanium showed greater increments in surface energy. All error bars are mean ± SEM; $n = 3$; *$p < 0.01$ (compared to flat) and **$p < 0.01$ (compared to nanometer).

improvement in RAEC attachment (more than 50% in Fig. 8c) [21,26].

4. Discussion

Although the importance of nano-technology has been stressed in various fields (including medical applications), the quantitative investigation of greater cell responses on nanometer and sub-micron features with identical chemistry remains unclear. This is because many previous studies have addressed altered cell responses on different feature sizes (micron to nanometer) and those surfaces also possessed altered chemistry. Thus, this makes it difficult to quantify the independent role of nanometer

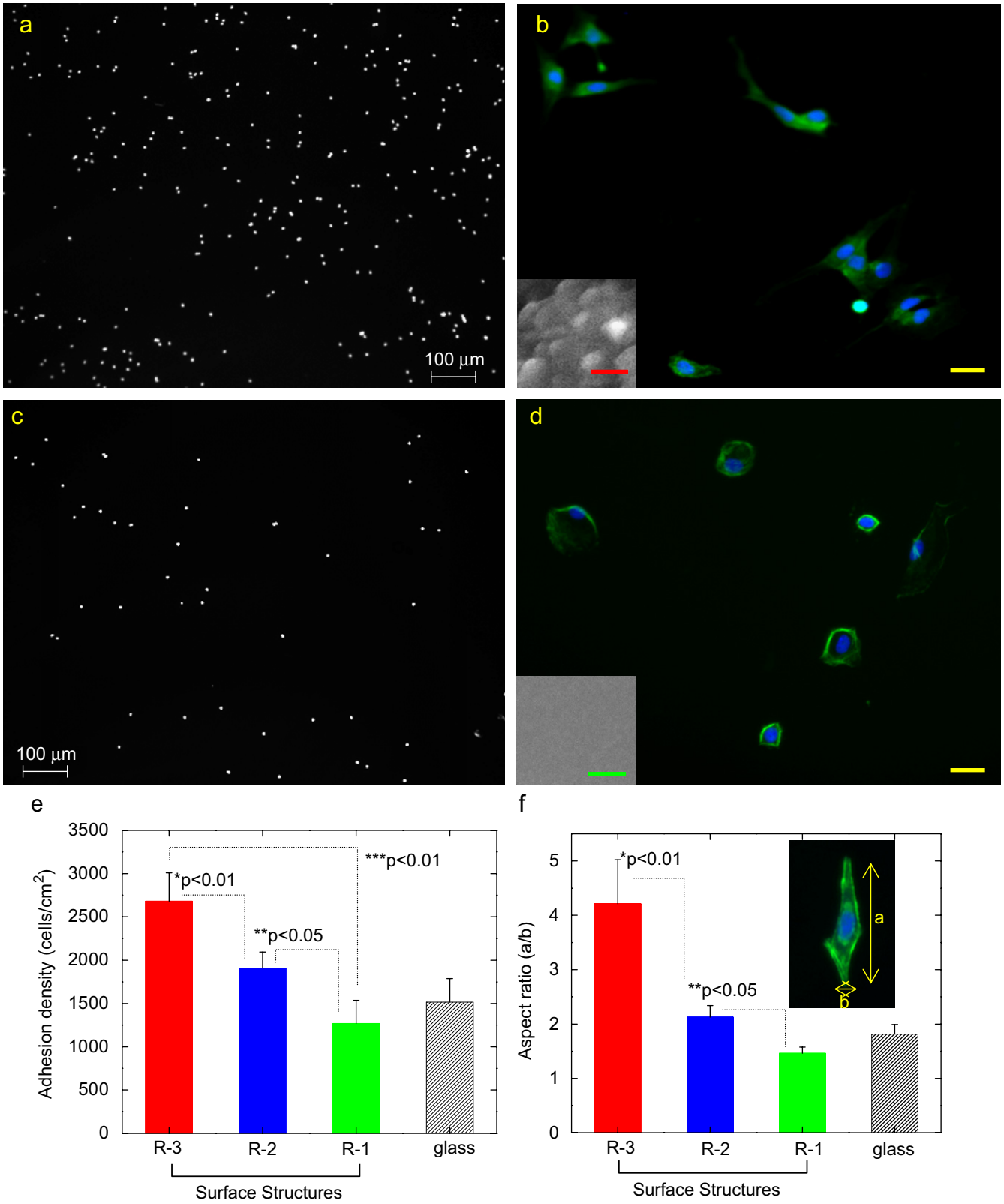

Fig. 5. RAEC adhesion on bulk substrates. (a) Fluorescence RAEC density on sub-micron structured surfaces (R-3). (b) Magnified fluorescence RAEC image of sub-micron surfaces showed high cell aspect ratios. Inset image shows SEM surface structures (bar is 100 nm). (c) Fluorescence RAEC density on flat surfaces (R-1). (d) Magnified fluorescence cell images of RAEC on flat surfaces show small cell aspect ratios (more round cellular shapes than on sub-micron surfaces. Bar is 100 nm). (e) Adhesion density showed that sub-micron structures led to the best adhesion density (seeding density was 3500 cells/cm^2). (f) Cell aspect ratios showed oriented cell morphology for flat, nanometer and sub-micron structures (increased right to left). Note that cell aspect ratios were calculated by the length of a single cell divided by its width (inset image of (f)). All error bars are mean $\pm$ SEM; $n = 3$; *$p < 0.01$ (compared to R-2) and **$p < 0.05$ (compared to R-1). All bars in (a) and (c) are 100 μm and bars in (b) and (d) are 20 μm.

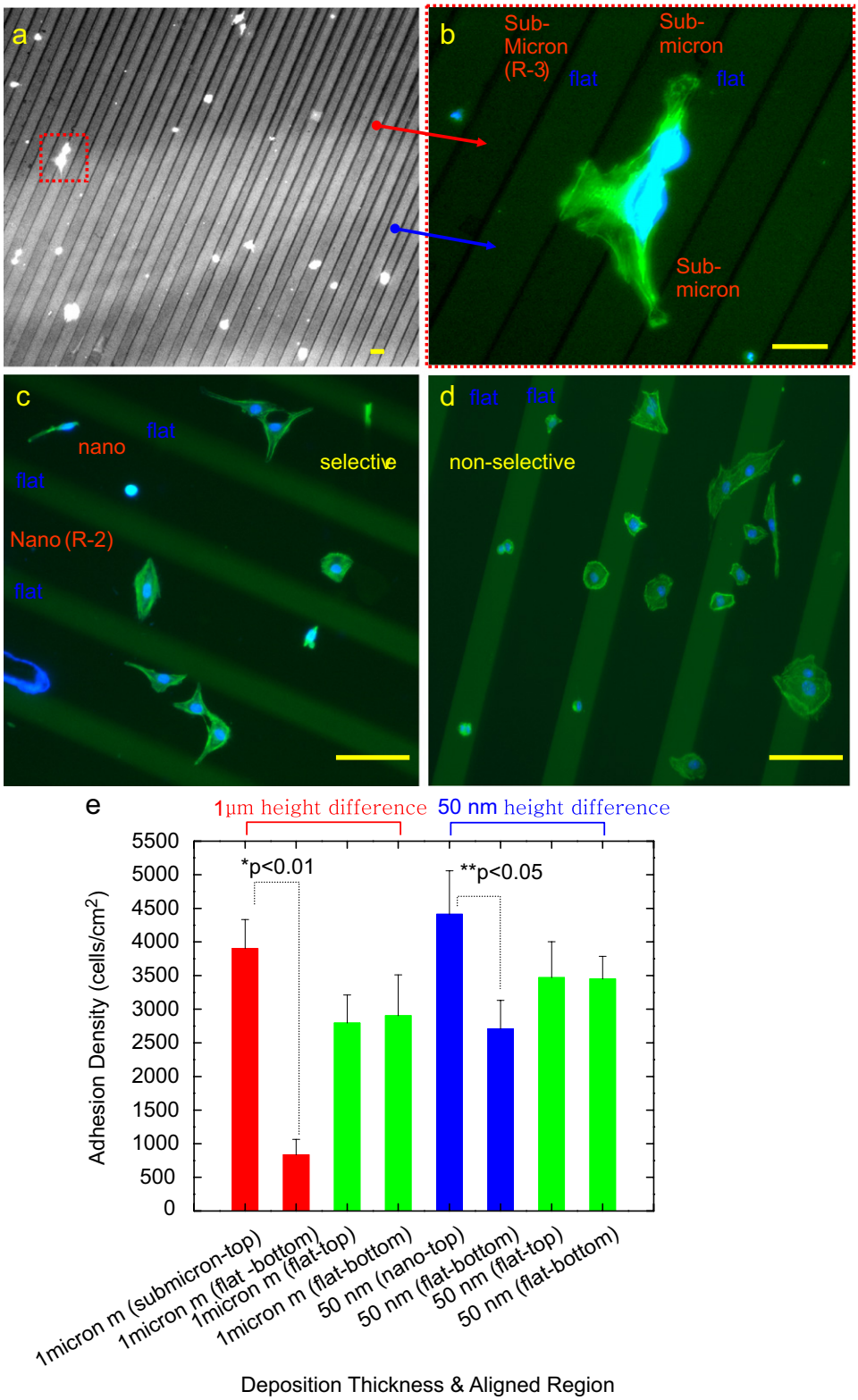

Fig. 6. Endothelial cell (RAEC) adhesion on aligned patterns. (a) Fluorescence cell image (nucleus: stained by Hoechst) showed selective RAEC adherent more on aligned sub-micron spaces (R-3) compared to aligned flat titanium (R-1). (b) Selected cell images (magnified) from (a) showed actin filaments oriented more on aligned sub-micron structured patterns than on aligned flat surface patterns. (c) Selective adhesion of endothelial cells showed more cells adherent on R-2 than R-1 (height was 50 nm). (d) Non-selective adhesion on the top layer (R-1) and bottom layer (R-1) showed no preferential attachment of RAEC cells. (e) Adhesion density of RAEC on different structured-layers. More than 80% of endothelial cells adhered on sub-micron structures but less than 20% of cells adhered on flat titanium surfaces. Nanometer surfaces also led to greater selective cell adhesion (more than 60%) than selective cell adhesion on flat surfaces (less than 40%). The height variation (1 μm and 50 nm) did not affect preferential cell adhesion on the top and bottom layers. All error bars are mean ± SEM; $n = 3$; *$p < 0.01$ (compared to the bottom layer) and **$p < 0.05$ (compared to the bottom layer). No significant p-values were observed for the flat top and flat bottom (both 50 nm and 1 μm height difference). Bars in (a), (c) and (d) are 60 nm. Bar in (b) is 20 nm.

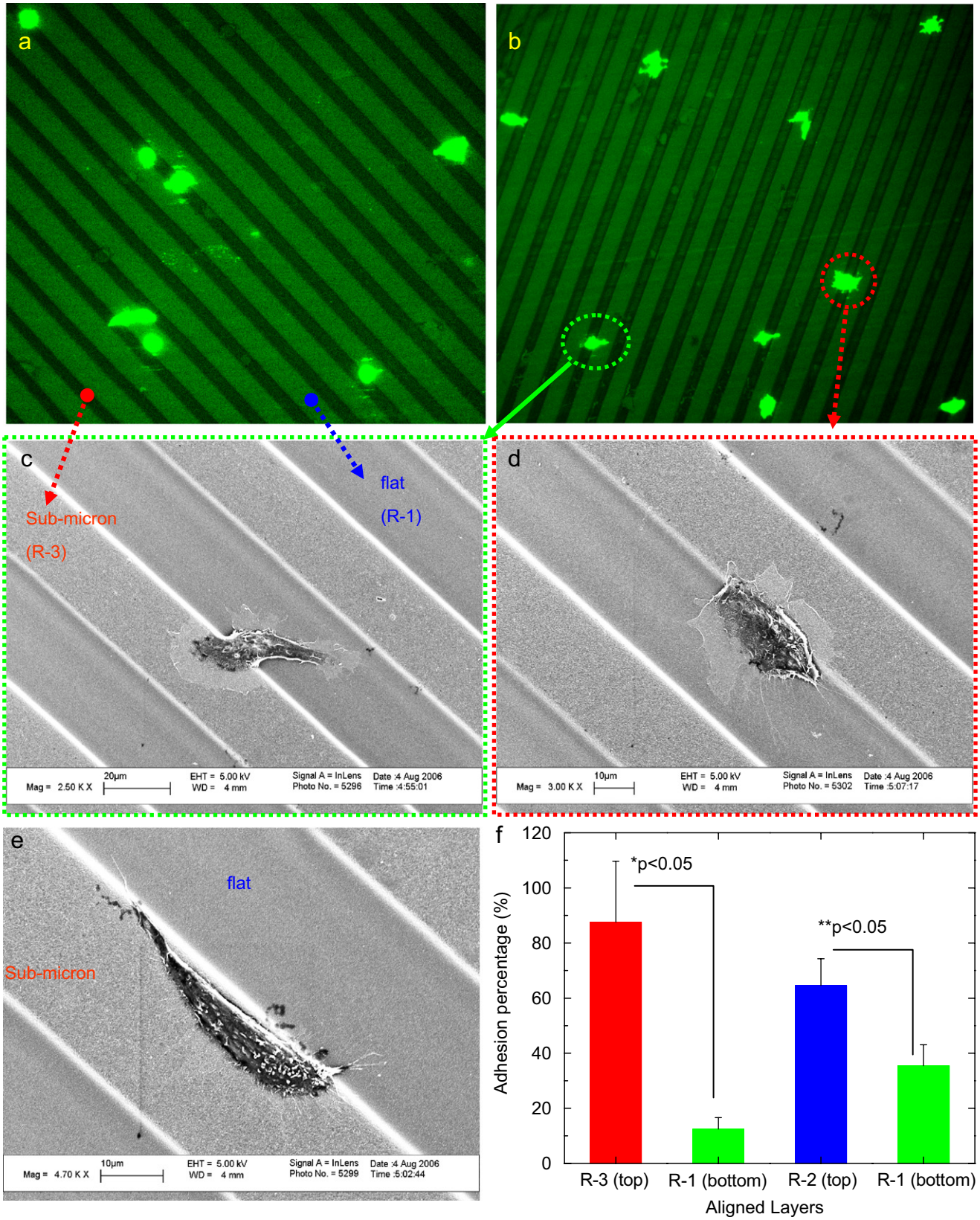

Fig. 7. Bone cell (HOB) adhesion on aligned patterns. Fluorescence live cell images, (a) and (b), showed that osteoblasts adhered more on sub-micron structures (R-3) than flat titanium (R-1) and, thus, provided evidence of selective responses of bone cells on sub-micron regions. The SEM images (c)–(e) indicated different cell adhesion. Note that some of the HOB adhered at the intersection sites (d) in which the intersection region included R-3 surface features with moderate increments of height as observed in Fig. 3e (not step structures). (f) HOB adhesion density analysis showed that both nanometer and sub-micron density led to selective adhesion compared to flat surfaces. Greater adhesion probability on sub-micron roughness than nanometer surfaces was observed. All error bars are mean $\pm$SEM; $n = 3$; $^{*}p < 0.01$ (compared to the bottom layer), and $^{**}p < 0.05$ (compared to the bottom layer).

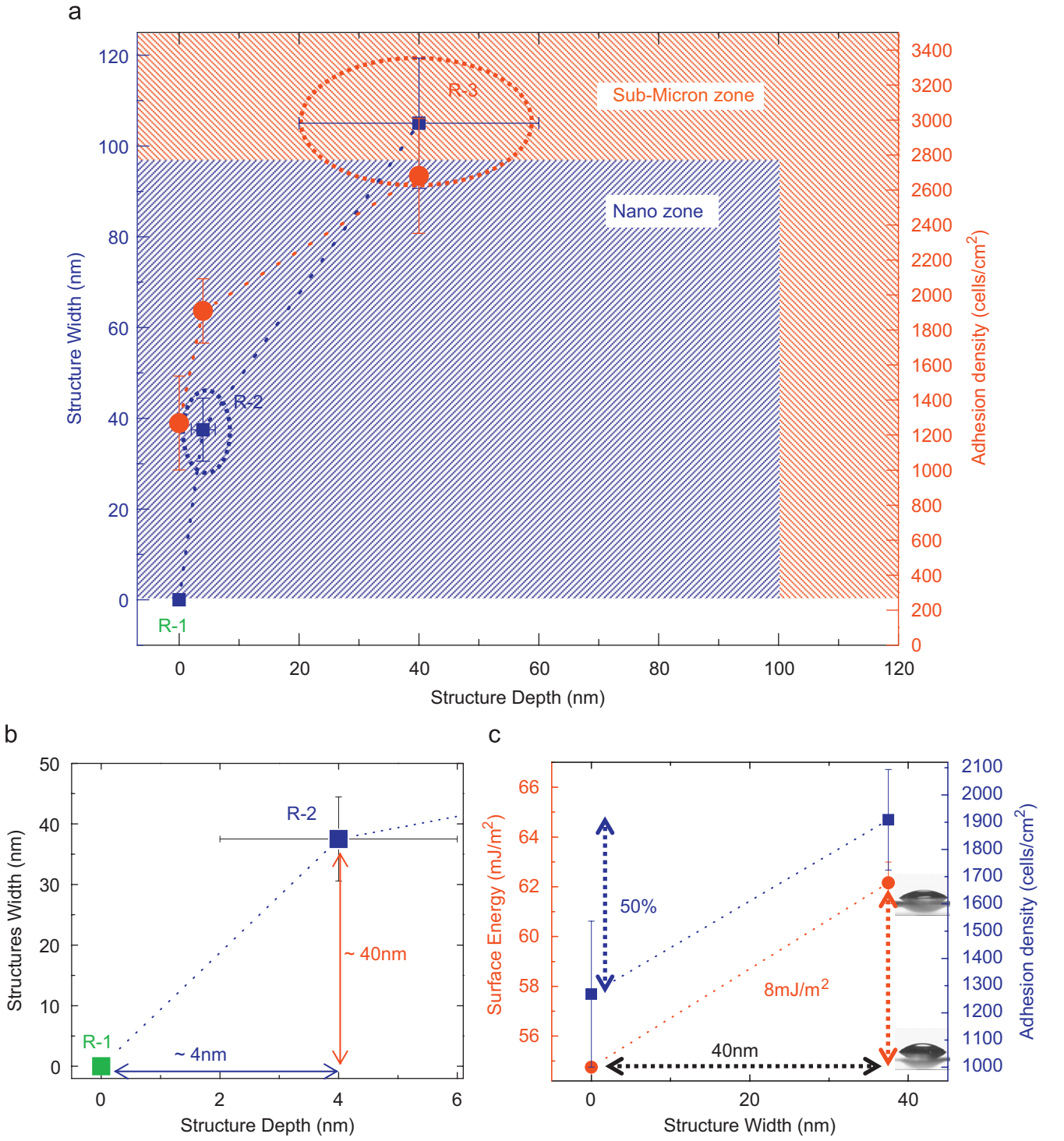

Fig. 8. Correlations between lateral width and depth versus RAEC adhesion: Importance of nanometer surface structures with respect to surface energy and cell adhesion. (a) RAEC adhesion on nanometer surface structures (less than 50 nm for both vertical and lateral scales) increased about 50% compared to flat (R-1) surfaces. Also, RAEC adhesion densities on sub-micron structures (R-3) increased about 200% compared to flat titanium. The cell adhesion difference between R-2 and R-3 was 40% (more cells on sub-micron than nanometer structures). Although vertical depths in sub-micron structures (R-3) were below 100 nm, a majority of R-3 features in the lateral dimension showed structures larger than 100 nm. Criteria of sub-micron and nanometer features were determined by the current definition of nano-technology involving dimensions less than 100 nm. (b) Vertical depth showed negligible differences between flat and nanometer titanium (4 nm) while lateral widths increased about 40 nm which is almost 10 times greater compared to the altered depth. (c) The importance of lateral nanometer surface features was stressed with respect to surface energy and cell adhesion. The 40 nm lateral structures led to both greater surface energy (8 mJ/m^2: corresponds to 10% increase in surface energy from flat titanium surface) and greater cell densities (50% increment for bone and endothelial cells).

and sub-micron structures on cell adhesion. In addition, all the vertical and lateral dimensions from nanometer and sub-micron surface features were fully analyzed here for the consideration of altered surface energy and subsequent cell adhesion. This is because the conventional RMS, a factor for measuring biomaterial surface roughness, is determined by vertical fluctuations from mean height values of structures, and is not a sufficient factor since it does not include information of altered lateral features on nanometer and sub-micron surfaces.

The main objective of this study was to delineate the importance of nanometer (50 nm in both lateral and vertical dimensions) and sub-micron titanium features (larger than 100 nm in lateral scale) of identical titanium chemistry on the adhesion of two tissue-forming cells (endothelial and bone).

Results of this study demonstrated that sub-micron structures showed the highest cytocompatibility properties for endothelial and bone cells. However, nanometer roughness showed the highest efficiency for both increasing surface energy and increasing cell adhesion compared to the altered width of surface features (about 40 nm).

Thus, all of these results collectively indicate the role of nanometer and sub-micron surface features (roughness) on the adhesion of endothelial and bone cells. Including the results from a previous study highlighting the role of nanometer surface roughness on polymers for promoting cell functions [22], this study suggested again an important design criteria concerning the contribution of nanometer surface features on titanium-based implant materials (for both vascular stents and orthopedic implants).

5. Conclusions

This study demonstrated that endothelial cells (cells on the interior surface of blood vessels) and osteoblasts (bone-forming cells) preferentially adhered onto both nanometer structured and sub-micron structured titanium surfaces compared to flat (smooth) titanium surfaces. To understand the correlation between nanometer and sub-micron-sized titanium structures and their initial cell adhesion on the same titanium chemistry, different sizes of surface features and aligned patterns on thin films were fabricated using an e-beam evaporator. Surface roughness (RMS) was controlled within the range 0–12 nm by altering deposition parameters (specifically, e-beam current density and deposition thickness). In addition, this study also demonstrated that nanometer (less than 100 nm in both the lateral and vertical dimension) and sub-micron (larger than 100 nm in the lateral dimension) surface structures drastically altered surface energy (one important factor that controls cell adhesion) without the modification of surface chemistry. Importantly, the individual role of sub-micron and nano-features in relation to the adhesion of endothelial and bone cells were quantified and results showed that these cells selectively adhered more on both sub-micron (400% increase) and nanometer (50% increase) surface structures than on flat surfaces.

Acknowledgments

This research was supported by the Coulter Foundation. The authors would like to thank Prof. Jay X. Tang (Department of Physics, Brown University) for assistance with AFM.

References

[1] Jayaraman M, Meyer U, Buhner M, Joos U, Wiesmann HP. Influence of titanium surfaces on attachment of osteoblast-like cells in vitro. Biomaterials 2004;25:625–31.
[2] Robertson SW, Imbeni V, Wenk HR, Ritchie RO. Crystallographic texture for tube and plate of the superelastic/shape-memory alloy nitinol used for endovascular stents. J Biomed Mater Res A 2005; 72A:190–9.
[3] Zhao G, Schwartz Z, Wieland M, Rupp F, Geis-Gerstorfer J, Cochran DL, et al. High surface energy enhances cell response to titanium substrate microstructure. J Biomed Mater Res A 2005;74A: 49–58.
[4] Farb A, Sangiorgi G, Carter AJ, Walley VM, Edwards WD, Schwartz RS, et al. Pathology of acute and chronic coronary stenting in humans. Circulation 1999;99:44–52.
[5] Lu J, Rao MP, MacDonald NC, Khang D, Webster TJ. Improved endothelial cell adhesion and proliferation on patterned titanium surfaces with rationally designed, micrometer to nanometer features. Acta Biomater 2008;4:192–201.
[6] Ball M, O'Brien A, Dolan F, Abbas G, McLaughlin JA. Macrophage responses to vascular stent coatings. J Biomed Mater Res A 2004; 70A:380–90.
[7] Choudhary S, Haberstroh KM, Webster TJ. Enhanced functions of vascular cells on nanostructured Ti for improved stent applications. Tissue Eng 2007;13:1421–30.
[8] American Academy of Orthopaedic Surgeons 2005; 〈http://www.aaos.org〉.
[9] de Aragon JSM, Keisu KS. 21-Year results of the uncemented fully textured lord hip prosthesis. Clin Orthop Relat Res 2007:133–8.
[10] Chacon GE, Stine EA, Larsen PE, Beck FM, McGlumphy EA. Effect of alendronate on endosseous implant integration: an in vivo study in rabbits. J Oral Maxillofac Surg 2006;64:1005–9.
[11] Davies JE. Mechanisms of endosseous integration. Int J Prosthodont 1998;11:391–401.
[12] Finke B, Luethen F, Schroeder K, Mueller PD, Bergemann C, Frant M, et al. The effect of positively charged plasma polymerization on initial osteoblastic focal adhesion on titanium surfaces. Biomaterials 2007;28:4521–34.
[13] Chung TW, Liu DZ, Wang SY, Wang SS. Enhancement of the growth of human endothelial cells by surface roughness at nanometer scale. Biomaterials 2003;24:4655–61.
[14] Webster TJ, Ejiofor JU. Increased osteoblast adhesion on nanophase metals: Ti, Ti6Al4V, and CoCrMo. Biomaterials 2004;25:4731–9.
[15] Kunzler TP, Drobek T, Schuler M, Spencer ND. Systematic study of osteoblast and fibroblast response to roughness by means of surface-morphology gradients. Biomaterials 2007;28:2175–82.
[16] Yao C, Slamovich EB, Webster TJ. Enhanced osteoblast functions on anodized titanium with nanotube-like structures. J Biomed Mater Res A 2007, in press (Available online).
[17] Zhao G, Raines AL, Wieland M, Schwartz Z, Boyan BD. Requirement for both micron- and submicron scale structure for synergistic responses of osteoblasts to substrate surface energy and topography. Biomaterials 2007;28:2821–9.

[18] Dyer MA, Ainslie KM, Pishko MV. Protein adhesion on silicon-supported hyperbranched poly(ethylene glycol) and poly(allylamine) thin films. Langmuir 2007;23:7018–23.
[19] Parkansky N, Alterkop B, Goldsmith S, Boxman RL, Wulff H, Quaas M, et al. Nano-organization of thin titanium films by an electrical field during vacuum arc deposition. Thin Solid Films 2000; 377:507–11.
[20] Toyoda N, Yamada I. Improvement of surface roughness by ultra-thin film deposition with oxygen cluster ion beam assist deposition. Mater Res Symp Proc 2003;749:W17.17.11–5.
[21] Liu X, Lim JY, Donahue HJ, Dhurjati R, Mastro AM, Vogler EA. Influence of substratum surface chemistry/energy and topography on the human fetal osteoblastic cell line hFOB 1.19: phenotypic and genotypic responses observed in vitro. Biomaterials 2007;28: 4535–50.
[22] Khang D, Kim SY, Liu-Snyder P, Palmore GTR, Durbin SM, Webster TJ. Enhanced fibronectin adsorption on carbon nanotube/poly(carbonate) urethane: independent role of surface nano-roughness and associated surface energy. Biomaterials 2007;28:4756–68.
[23] Chow TS. Wetting of rough surfaces. J Phys: Condens Matter 1998; 10:L445–51.
[24] McHale G, Shirtcliffe NJ, Aqil S, Perry CC, Newton MI. Topography driven spreading. Phys Rev Lett 2004:93.
[25] Washburn NR, Yamada KM, Simon CG, Kennedy SB, Amis EJ. High-throughput investigation of osteoblast response to polymer crystallinity: influence of nanometer-scale roughness on proliferation. Biomaterials 2004;25:1215–24.
[26] Pesakova V, Kubies D, Hulejova H, Himmlova L. The influence of implant surface properties on cell adhesion and proliferation. J Mater Sci-Mater Med 2007;18:465–73.